Article:
Kusins, J., Knowles, N., Ryan, M. et al. (2019) Performance of QCT-Derived scapula finite element models in predicting local displacements using digital volume correlation. Journal of the Mechanical Behavior of Biomedical Materials, 97. pp. 339-345. ISSN: 1751-6161

https://doi.org/10.1016/j.jmbbm.2019.05.021

Performance of QCT-Derived Scapula Finite Element Models in Predicting Local Displacements Using Digital Volume Correlation

Jonathan Kusins[1,2], Nikolas Knowles[1,2], Melissa Ryan[3,4], Enrico Dall'Ara[3,4], Louis Ferreira[1,2,*]

[1]Department of Mechanical and Materials Engineering
Western University
London, Canada

[2]Roth|McFarlane Hand and Upper Limb Centre
St. Joseph's Health Care
London, Canada

[3]Department of Oncology and Metabolism
University of Sheffield
Sheffield, United Kingdom

[4]Insigneo Institute for In Silico Medicine
University of Sheffield
Sheffield, United Kingdom

***Correspondence Address:**

Louis M. Ferreira, PhD
Roth|McFarlane Hand and Upper Limb Centre,
Surgical Mechatronics Laboratory, St. Josephs Health Care,
268 Grosvenor St. London, ON, Canada.
Tel: +1 519 646 6000 X. 61351
E-mail address: Louis.Ferreira@sjhc.london.on.ca

Keywords: Subject-specific finite element analysis; digital volume correlation; shoulder FEM; CT-compatible loading.

Abstract

Subject-specific finite element models (FEMs) of the shoulder complex are commonly used to predict differences in internal load distribution due to injury, treatment or disease. However, these models rely on various underlying assumptions, and although experimental validation is warranted, it is difficult to obtain and often not performed. The goal of the current study was to quantify the accuracy of local displacements predicted by subject-specific QCT-based FEMs of the scapula, compared to experimental measurements obtained by combining digital volume correlation (DVC) and mechanical loading of cadaveric specimens within a microCT scanner.

Four cadaveric specimens were loaded within a microCT scanner using a custom-designed six degree-of-freedom hexapod robot augmented with carbon fiber struts for radiolucency. BoneDVC software was used to quantify full-field experimental displacements between pre- and post-loaded scans. Corresponding scapula QCT-FEMs were generated and three types of boundary conditions (BC) (idealized-displacement, idealized-force, and DVC-derived) were simulated for each specimen.

DVC-derived BCs resulted in the closest match to the experimental results for all specimens (best agreement: slope ranging from 0.87 - 1.09; highest correlation: r^2 ranging from 0.79-1.00). In addition, a two orders of magnitude decrease was observed in root-mean-square error when using QCT-FEMs with simulated DVC-derived BCs compared to idealized-displacement and idealized-force BCs.

The results of this study demonstrate that scapula QCT-FEMs can accurately predict local experimental full-field displacements if the BCs are derived from DVC measurements.

1. Introduction

Subject-specific finite element models (FEMs) of the shoulder complex provide the capability to predict the internal load distribution of the joint. Although quantitative computed tomography (QCT)-derived FEMs have been accepted as an established research tool to further understand the mechanics of the shoulder (Allred et al., 2016; Terrier et al., 2005; Zheng et al., 2017), the accuracy of predictions generated by these models is to some extent unknown. Currently, experimental validation of QCT-FEMs of the shoulder is limited to localized predictions of strain on the cortical shell (Dahan et al., 2016; Gupta et al., 2004); while the accuracy of internal predictions within the trabecular bone has yet to be explored.

To observe the internal load distribution within human bone, recent experimental protocols have combined mechanical loading with simultaneous time-lapsed volumetric imaging of bone specimens undergoing deformation (Nazarian and Müller, 2004). Digital volume correlation (DVC) techniques have been introduced to quantify full-field localized displacement measurements between pre- and post-loaded volumetric images (Grassi and Isaksson, 2015; Roberts et al., 2014). In addition, previous experimental studies that have combined volumetric imaging with DVC analysis techniques have shown great promise to elucidate internal fracture mechanisms by quantifying progressive strain and damage evolution within composite materials (Croom et al., 2016, 2019, 2017). To acquire volumetric images of a deformed specimen, a CT-compatible loading device is required. Current CT-compatible joint loading devices are based on screw-type mechanisms and are restricted by the degrees-of-freedom (dof) of load they can apply (Du et al., 2015; Jackman et al., 2016; Martelli and Perilli, 2018; Palanca et al., 2016; Sukjamsri et al., 2015; Zhou et al., 2018). However, to properly replicate physiological joint loads at the shoulder complex, a 6-dof loading mechanism would be desirable. Regardless, current

78 experimental protocols developed with DVC techniques have shown tremendous promise by
79 quantifying internal localized deformations within trabecular bone that otherwise cannot be
80 captured experimentally (Bay et al., 1999; Chen et al., 2017; Gillard et al., 2014; Liu and Morgan,
81 2007).

82 DVC has been applied at the micro (*e.g.* trabecular bone cores) and joint level (*e.g.*
83 vertebra) to validate μCT- and QCT-FEMs respectively (Chen et al., 2017; Costa et al., 2017;
84 Hussein et al., 2018; Jackman et al., 2016; Mao et al., 2019, p.; Zauel et al., 2005). At the micro
85 level, the accuracy of the predictions generated by μCT-FEMs was found to be sensitive to the
86 boundary condition (BC) modelled (Chen et al., 2017). Specifically, when using BCs derived
87 directly from local DVC measurements, any inherent experimental limitations (*e.g.* specimen
88 fixation rigidity or structural stiffness of the loading mechanism) were assumed to be eliminated
89 and thus excellent agreement (slope (m) ≈ 1, coefficient of determination (r^2) ≈ 1, y-intercept (b)
90 ≈ 0) was achieved (Chen et al., 2017; Costa et al., 2017; Oliviero et al., 2018). However, when
91 extrapolating these techniques to QCT-FEMs at the joint level, similar success has not been
92 reported. Previous studies performed by Jackman *et. al.* and Hussein *et. al.* within the vertebra
93 found improvements in performance of QCT-FEMs when using BCs derived from DVC
94 measurements obtained at the yield point; but only moderate agreement between the experimental
95 local displacements and FEM predictions were observed (Hussein et al., 2018; Jackman et al.,
96 2016). A similar validation study has yet to be performed to quantify the performance of shoulder
97 QCT-FEMs in predicting local experimental displacement measurements obtained through DVC.

98 Hence, the primary objective of the current study was to quantify the accuracy of local
99 displacements predicted by subject-specific shoulder QCT-FEMs compared to experimental
100 measurements obtained through mechanical loading and simultaneous volumetric imaging of

cadaveric scapular specimens. A secondary objective was the design and fabrication of a CT-compatible 6-dof loading apparatus capable of applying articular loads within a microCT scanner.

2. Materials and Methods

2.1 Development of a CT-Compatible 6-DOF Loading Apparatus

A custom 6-dof hexapod parallel robot was designed to apply external loads to a scapula. The robot consisted of a base, loading platform and six prismatic actuators that connected the base and platform (Figure 1) in a configuration consistent with a Stewart platform design. Although variations exist, the Stewart platform design commonly uses six linear actuators attached in pairs by universal joints to a movable platform and fixed base. Each prismatic actuator is composed of a lead screw mechanism driven by independent servo-motors. Although the robot consisted of only linear actuators, its hexapod configuration transforms linear displacements into complete 6-dof motions that include all possible translations and rotations, within its range of motion. In addition, the Stewart platform design is noted to have a high load carrying capacity within a small working envelope and has been used in previous applications involving 6-dof biomechanical testing applications (Boyin Ding et al., 2011; Lawless et al., 2014; Walker and Dickey, 2007).

The hexapod robot was augmented with radiolucent carbon fiber extensions to provide CT-compatibility with a Nikon XT H 225ST cone-beam microCT scanner. Custom fixtures were fabricated to allow for loads to be applied to the glenoid of a cadaveric scapula within a microCT scanner. A hemispherical platen (diameter equal to 48 mm) was fabricated from acetal plastic and attached to the loading platform via an acrylic extension rod. A 6-dof load cell (Mini 45, ATI Industrial Automation, NC, USA) was instrumented to the loading platform to provide real-time

force feedback during the experimental loading protocol. Overall, the current system can apply 1.5 kN of compression and weighs 9.6 kg.

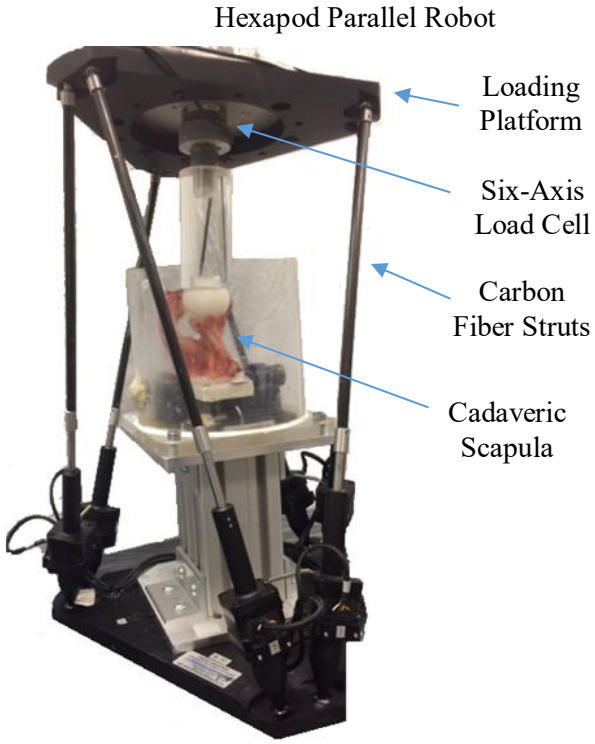

Figure 1: A custom-designed six degree-of-freedom hexapod robot was used to experimentally load cadaveric scapulae within a cone-beam microCT scanner. The use of carbon fiber struts provided radiolucent sections to reduce any imaging artifacts that may occur with use of the hexapod robot.

2.2 Specimen Preparation and Experimental Loading

Four cadaveric shoulders (two male and two female) were tested (Table 1). Prior to experimental loading, the specimens with soft tissue intact were imaged within a clinical QCT-scanner (GE Discovery CT750 HD, Milwaukee, WI, USA) at clinical scan settings (pixel size: 0.625 mm to 0.668 mm, slice thickness: 0.625 mm, 120 kVp, 200 mA, BONEPLUS). A dipotassium phosphate (K_2HPO_4) calibration phantom (QCT Pro, Mindways Software Inc., Austin, TX, USA) was included in each QCT scan for specimen-specific QCT-density relationships. QCT scans obtained

at clinical resolution were used for development of continuum-level QCT-derived finite element models described further in Section 2.4. Following the scanning protocol, each scapula was denuded of all soft tissue. The glenoid articular surface was resurfaced using a clinical shoulder reaming tool to provide a consistent uniform surface for experimental loading. The scapula was then cut on a medial plane (sectioned approximately 55 mm from the articular surface) and cemented in polymethyl methacrylate (PMMA) for fixation in the hexapod robot. A custom jig was used to orient the axis at which the glenoid was resurfaced perpendicular to the loading platform of the hexapod robot.

Table 1: Age, sex, and QCT density (±1 SD) of cadaveric scapulae specimens.

	Sex	Age	QCT Density (g_{K2HPO4}/cm^3)
Specimen 1	Male	80	0.333 ± 0.256
Specimen 2	Male	73	0.245 ± 0.198
Specimen 3	Female	62	0.376 ± 0.240
Specimen 4	Female	52	0.377 ± 0.253

Experimental loading for each scapula was performed within a cone-beam microCT scanner (Nikon XT H 225ST). Each specimen was wrapped with tissue-soaked phosphate-buffered saline solution to ensure hydration throughout the scanning protocol. The hexapod robot, previously described, was used to apply external loads. Consistent for each specimen, an initial stabilizing load (10 N, settling time of 20 minutes to allow for specimen relaxation) was applied and a pre-loaded microCT scan was acquired (33.5 μm isotropic voxel size, 95 kVp, 64 μA, 3141 projections, 55 minute scan time, 1000 ms exposure). Two post-loaded scans of the specimen were then obtained with identical settings as the pre-loaded scan. The first load consisted of a target compressive load of 500 N with a settling time of 20 minutes. The second load consisted of a target 500 N load applied off-axis, 5° posterior for each specimen and 5° inferior for specimens 1, 2, and 4 with respect to the robot's frame. An inferior off-axis angle was not applied to specimen 3 due

to interference between the acrylic extension rod and the acromion of the specimen. Both loading cases were performed directly within the microCT scanner, without repositioning the loading apparatus between scans. Load cell measurements were acquired via a NI-USB 6210 data acquisition unit (National Instruments Corporation, Austin, Texas) obtained after the 20 minutes settling time but prior to the microCT scan. The resulting field of view (FOV) for each scan was a cube with edge lengths of 65 mm, which captured the glenoid vault (approximately 25 mm medial from the articular surface) and the loading platen in the pre- and post-loaded states.

2.3 Digital Volume Correlation

Local experimental displacement measurements between the pre- and post-loaded images were obtained using DVC algorithms (Figure 2). To prepare the images for DVC, a specimen-specific threshold was applied (Mimics v.20.0, Materialise, Leuven, BE) to segment and isolate the glenoid vault from other objects captured within the microCT scans (*e.g.* loading platen). Values outside the selected threshold were assigned a constant grey level value similar to bone marrow (equivalent to 85 in 8-bit greyscale). The images were then cropped and converted to 8-bit greyscale (ImageJ, NIH) (Schneider et al., 2012).

A previously established and validated deformable image registration toolkit, BoneDVC, was used to quantify the full-field experimental displacement field between the pre- and post-loaded images (Dall'Ara et al., 2017, 2014). BoneDVC is a global based DVC approach that computes full-field local displacement vectors between two sets of volumetric images using cross correlation techniques (Dall'Ara et al., 2014). Furthermore, BoneDVC has previously been used to validate μFEMs for various osseous structures (Chen et al., 2017; Costa et al., 2017; Oliviero et al., 2018). To compute the precision of the local displacement measurements quantified by

BoneDVC, a standard procedure of comparing two pre-loaded scans with various nodal spacing was performed (Dall'Ara et al., 2017, 2014). Based on these results, a nodal spacing of 30 voxels, (approximately 1 mm), was decided as an optimal tradeoff between spatial resolution and precision (error along x, y, and z direction lower than 2.5 µm).

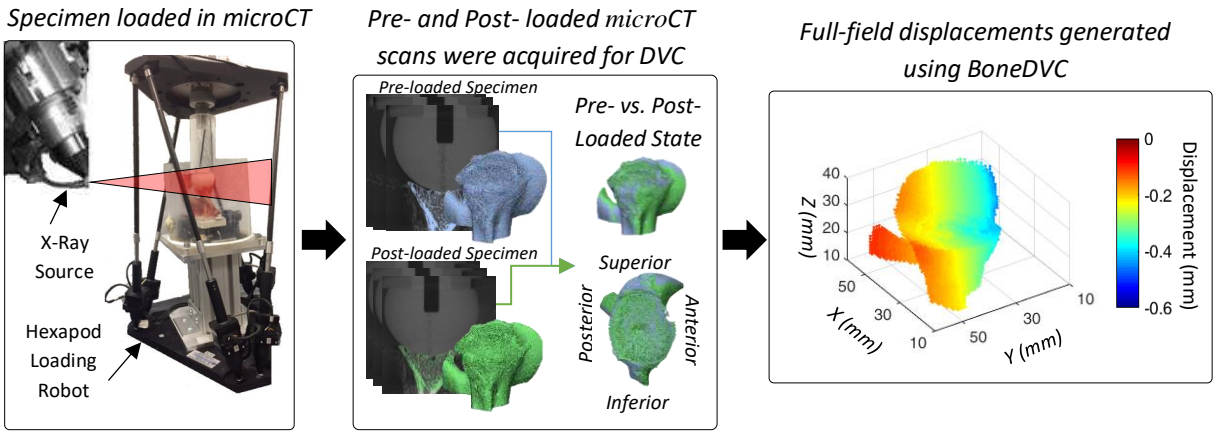

Figure 2: Four scapula specimens were scanned within a microCT at a resolution of 33.5 µm in pre- and post-loaded states. Full-field local displacements (sub-volume size ≈ 1 mm) between the pre- and post-loaded scans were obtained using BoneDVC.

2.4 Computational In-Silico Modelling

Specimen-specific QCT-FEMs were generated for each scapula to simulate the experimental loading set-up. The geometry of each scapula was extracted from the corresponding QCT scan acquired prior to experimental loading. To identify the medial border at which the experimental scapulae were cut, laser surface scans (Artec Spider, Artec 3D, Luxembourg) were acquired for each prepared specimen. From these, STL models were generated and registered to the QCT models. Anything below the PMMA surface was removed by Boolean subtraction. In addition, any elements within the volume of the reamed articular surface were removed to match the prepared cadaveric scapulae. A surface triangular mesh was generated (3-matic v.12.0, Materialise, Leuven, BE) with a target edge length of 1 mm (Burkhart et al., 2013). The surface

mesh was then converted to a quadratic tetrahedral mesh using ABAQUS (v.6.14, Simulia, Providence, RI). Linear elastic isotropic material properties were applied to the volumetric mesh (Mimics v.20.0, Materialise, Leuven, BE) based on the local density measure using Eq.1 and Eq. 2 (Rice et al., 1988; Schaffler and Burr, 1988).

$$\rho_{app} < 1.54 \text{ g/cm}^3 \qquad E_{trab} = 60 + 900 * {\rho_{app}}^2 \qquad \text{(Eq. 1)}$$

$$\rho_{app} \geq 1.54 \text{ g/cm}^3 \qquad E_{cort} = 90 * {\rho_{app}}^{7.4} \qquad \text{(Eq. 2)}$$

Where E_{trab} is Young's modulus of trabecular bone [MPa], E_{cort} is Young's modulus of cortical bone [MPa], and ρ_{app} is apparent density.

To register the QCT-FEMs to the coordinate system of the microCT, an iterative closest points algorithm (3-matic Research 11.0, Materialise, Leuven, BE) was performed aligning the outer geometry of the QCT-derived scapula to the corresponding microCT-derived scapula (Knowles et al., 2019).

Three separate boundary conditions (BCs) were modelled (ABAQUS v.6.14, Simulia, Providence, RI) to investigate their effect on the accuracy of the QCT-FEMs. The first two simulations consisted of idealized BCs (idealized-displacement BC and idealized-force BC). For both idealized BCs, a deformable virtual loading platen, meshed with hexahedral elements (E = 3100 MPa, ν = 0.35), was constructed and general contact between the virtual platen and scapula was modelled (coefficient of friction = 0.2). The medial border of the scapula was assumed to be fixed and either a force (idealized-force BC) or displacement (idealized-displacement BC) was applied to the virtual loading platen (Figure 3). For the idealized-force BC, the experimental force measured immediately prior to the microCT scan was prescribed to the top nodes of the virtual loading platen. For the idealized-displacement BC, a displacement was prescribed to the top nodes of virtual loading platen forcing the platen to the post-loaded experimental position. The

experimental post-loaded position of the loading platen was quantified by segmenting out the experimental platen in the corresponding raw post-loaded microCT image.

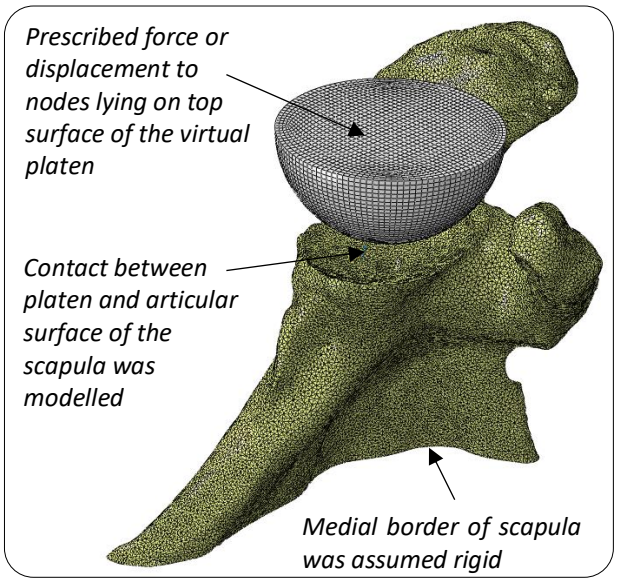

Figure 3: Specimen-specific QCT-FEMs with idealized BCs were modelled. Idealized BCs assumed the medial border of the scapula was fixed and either a displacement (idealized-displacement) or force (idealized-force) was applied to the virtual loading platen.

In addition, DVC-derived BCs were modelled (Chen et al., 2017; Costa et al., 2017; Jackman et al., 2016; Zauel et al., 2005) (Figure 4). First, to generate the DVC-derived BCs, each specimen was further cropped medially due to the limited FOV of the microCT scans. Subsequently, local displacements were prescribed to each node lying on the articular surface of the glenoid and the medial surface of the cropped scapula. A custom Matlab code (v.R2017a, Mathworks, Natick, MA) applied tri-linear interpolation to local displacements provided by the DVC measurements onto the corresponding QCT-FEM nodes.

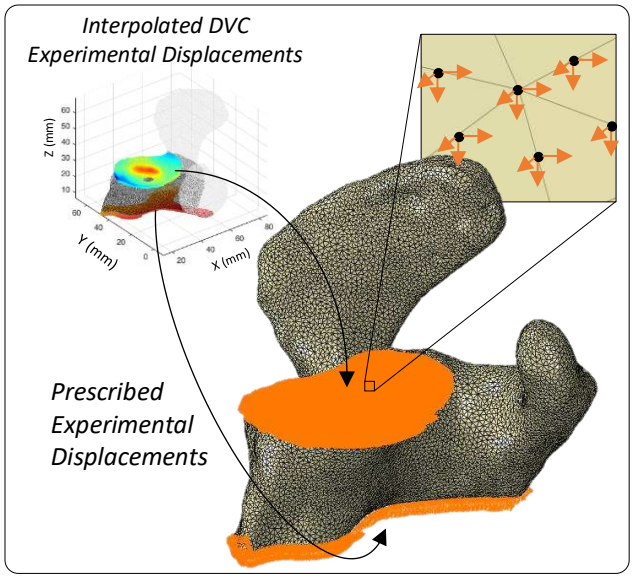

Figure 4: DVC-derived BCs were modelled by assigning local experimental displacements obtained by DVC directly to the articular and medial surface of the QCT-FEM scapula.

2.5 Statistical Analysis

To quantify the performance of the scapula QCT-FEMs, local displacement predictions were compared to DVC experimental measurements using linear regression. To pair the outcome measures, local DVC displacements were paired with averaged QCT-FEM predicted displacements, region averaged within a 1mm cubic voxel, equivalent to the DVC nodal spacing and dependent on the nodal location of the DVC measurement (Hussein et al., 2018; Jackman et al., 2016). Furthermore, to exclude any measurements prescribed by the DVC-derived BCs, only nodes within the middle 80% of the scanned specimen were used for comparison. Outliers were removed from the paired QCT-FEM predictions and local DVC results along the x, y, and z direction using 5x the Cook's distance (Costa et al., 2017). Slope (m), coefficient of determination (r^2) and root-mean-square error (RMSE) were quantified for both loading conditions (compressive and off-axis) and with each BC (idealized-force, idealized-displacement, and DVC-derived).

In addition, reaction forces predicted by the QCT-FEMs with idealized-displacement BCs and DVC-derived BCs were compared to the experimental applied force. Idealized-force BCs was not included, as the input force required to generate the model was equal to the experimentally measured force. Absolute percentage error was quantified for each specimen and for both loading cases.

3. Results

The accuracy of predictions generated by the QCT-FEMs was found to be highly sensitive to the boundary conditions simulated. For all four specimens subjected to the compressive load, the performance of QCT-FEMs in predicting experimental local displacements were vastly improved with DVC-derived BCs (Table 2, Figure 5). DVC-derived BCs resulted in the closest match to the experimental results, with ranges of m = 0.93 – 1.05, b = -0.02 – 0.01, and r^2 = 0.83 – 1.00 for each specimen along the x, y, and z direction. Similar agreement between the experimental and QCT-FEM predictions were not obtained when using idealized BCs. High variations within m (-0.13 – 1.66), b (-0.09 – 0.28) and r^2 (0.002 – 0.93) were observed for QCT-FEMs with idealized-force BCs. In addition, high variations in m (-0.03 – 2.84), b (-0.29 – 0.75), and r^2 (0.001 – 0.95) were observed when using idealized-displacement BCs for all specimens. Overall, RMSE was decreased by two orders of magnitude when using DVC-derived BCs (average RMSE of 4.1±0.9 µm, 4.7±2.2 µm, 4.8±2.3 µm along x, y, and z direction respectively) compared to the idealized-force BC (average RMSE of 414±479 µm, 401±356 µm, 331±170 µm along x, y, and z direction respectively) and idealized-displacement BC (average RMSE of 367±342 µm, 322±273 µm, 175±96 µm along x, y, and z direction respectively).

Table 2: Linear regression results between local displacements predicted by QCT-based FEMs and DVC experimental results due to a compressive load.

		Slope (m)			y-intercept (b)			Coefficient of Correlation (r^2)			Root Mean Square Error (RMSE) (μm)		
Specimen #		x	y	z	x	y	z	x	y	z	x	y	z
Idealized-Force BC	1	0.52	0.21	0.11	0.12	0.08	0.00	0.89	0.38	0.10	237	447	234
	2	-0.02	-0.10	-0.13	0.00	0.07	-0.09	0.01	0.59	0.47	37	866	565
	3	0.01	0.31	0.10	0.02	-0.07	-0.02	< 0.01	0.50	0.48	1117	274	248
	4	1.05	1.66	0.88	0.28	-0.01	0.17	0.93	0.82	0.77	265	18	199
Idealized-Displacement BC	1	2.84	1.00	0.54	0.66	0.39	-0.02	0.95	0.37	0.06	211	398	158
	2	-0.03	0.17	0.08	-0.11	0.05	-0.29	< 0.01	0.01	< 0.01	126	655	299
	3	0.90	0.96	1.01	0.75	-0.20	0.06	0.48	0.16	0.94	873	223	66
	4	1.39	1.69	1.65	0.38	0.00	0.31	0.85	0.62	0.82	258	12	178
DVC-Derived BC	1	1.00	0.99	1.01	0.00	-0.01	0.00	0.97	0.98	0.99	4.9	6.7	6.4
	2	0.99	0.99	1.00	0.00	0.01	0.00	0.99	1.00	1.00	2.9	2.5	2.5
	3	0.99	1.05	1.02	-0.01	-0.02	0.00	1.00	0.95	1.00	4.7	6.5	7.3
	4	0.93	0.93	1.02	-0.02	0.00	0.00	0.97	0.83	0.99	3.6	3.1	3.2

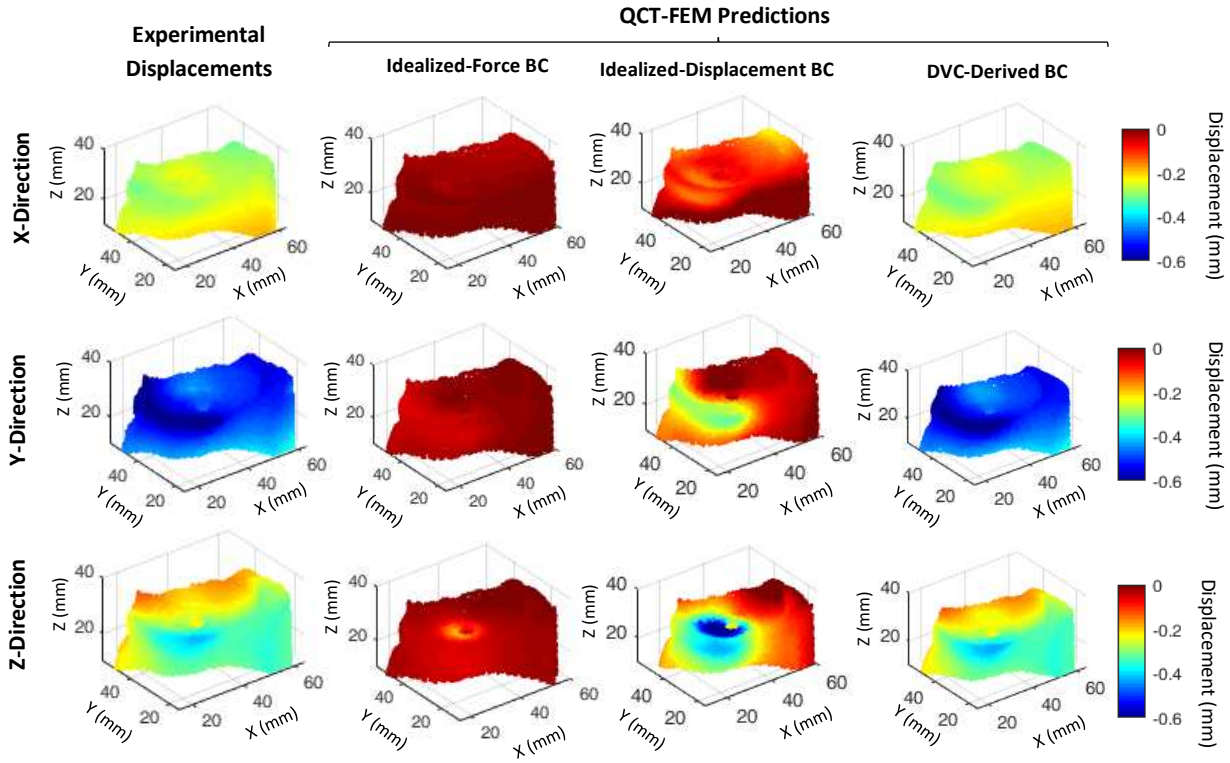

Figure 5: Representative full-field experimental displacements for specimen 1 during a compressive load, compared to predictions generated by a QCT-FEM with idealized-force BC, idealized-displacement BC, and DVC-derived BC.

For the off-axis load, similar results to the compressive load were observed (Table 3). High variability in m (ranges -0.40 – 2.35), b (-0.70 – 0.98), and r^2 (0.002 – 0.98) were observed for both idealized BCs. However, when using DVC-derived BCs, excellent agreement with the experimental results were obtained with ranges of m (0.87 – 1.09), b (-0.03 – 0.03), and r^2 (0.79 – 1.00) for each specimen. In addition, RMSE between the QCT-FEM predictions and experimental measurements was greatly reduced when using DVC-derived BCs (average RMSE of 4.8±0.7 µm, 5.3±1.0 µm, 6.0±1.4 µm along x, y, and z direction) compared to idealized-force BC (average RMSE of 541±268 µm, 443±681 µm, 337±225 µm along x, y, and z direction) and idealized-displacement BC (average RMSE of 494±343 µm, 345±484 µm, 196±147 µm along the x, y, and z direction).

Table 3: Linear regression results between local displacements predicted by QCT-based FEMs and DVC experimental results due to an off-axis load.

		Slope (m)			y-intercept (b)			Coefficient of Correlation (r^2)			Root Mean Square Error (RMSE) (µm)		
Specimen #		x	y	z	x	y	z	x	y	z	x	y	z
Idealized-Force BC	1	-0.04	-0.40	0.53	-0.01	0.14	0.09	< 0.01	0.08	0.74	311	110	185
	2	-0.07	-0.02	-0.05	-0.03	0.03	-0.05	0.55	0.14	0.31	719	1460	670
	3	0.79	0.90	0.80	0.57	-0.15	0.20	0.98	0.92	0.98	822	175	260
	4	0.68	1.20	0.61	0.20	-0.03	0.13	0.89	0.68	0.66	311	28	230
Idealized-Displacement BC	1	0.47	0.32	1.53	0.16	0.09	0.24	0.09	0.02	0.84	322	66	139
	2	0.86	0.75	0.78	0.29	-0.70	0.25	0.75	0.80	0.74	394	1063	405
	3	0.99	0.89	1.18	0.98	-0.19	0.06	0.43	0.07	0.93	1001	233	62
	4	2.13	2.35	2.27	0.64	-0.03	0.48	0.84	0.60	0.79	259	35	177
DVC-Derived BC	1	1.03	1.05	1.05	0.01	-0.01	0.01	0.96	0.98	0.99	4.2	4.4	6.6
	2	0.98	0.98	1.00	-0.02	0.03	0.00	0.99	1.00	1.00	5.8	5.0	5.0
	3	0.99	1.09	1.01	-0.01	-0.03	0.00	1.00	0.95	1.00	4.9	6.7	7.8
	4	1.03	0.87	1.00	0.01	0.00	0.00	0.97	0.79	0.98	4.2	5.1	4.8

High percentage errors (average error = 333%, range = 169 - 429%) in reaction forces were required to displace the virtual loading platen when using idealized-displacement BCs. Comparatively, the percentage error was reduced when using QCT-FEMs with DVC-derived BCs (average error = 32%, range = 8 - 44%). Similar results were observed with an off-axis load, with

higher percentage errors when using idealized-displacement BCs (average error = 350%, range = 152 - 520%) compared to DVC-derived BCs (average error = 26%, range = 6 - 50%).

4. Discussion

The goal of the current study was to quantify the performance of scapula QCT-FEMs in predicting local displacement measurements obtained from combining digital volume correlation (DVC) and mechanical loading within a microCT scanner. Due to the inability to resolve trabecular microarchitecture at a resolution associated with clinical *in-vivo* imaging of bone, QCT-FEMs rely on continuum-level assumptions and ignore the geometry of the inner trabecular network. However, the accuracy of local predictions generated by subject-specific vertebra QCT-FEMs has recently been questioned (Hussein et al., 2018; Jackman et al., 2016). The results of the current study found that QCT-FEMs of the scapula can accurately predict local displacement measurements when using DVC-derived BCs. A two orders of magnitude decrease was observed in RMSE, when using QCT-FEMs with simulated DVC-derived BCs compared to the idealized BCs during a compressive or off-axis load. Furthermore, excellent agreement (m ranging from 0.87 - 1.09, r^2 ranging from 0.79 - 1.00) was found between experimental results and QCT-FEM predictions when using DVC-derived BCs, consistent with previous studies performed using μ-FEMs on different bone structures (Chen et al., 2017; Costa et al., 2017; Oliviero et al., 2018). Reaction forces predicted by the QCT-FEMs with DVC-derived BCs were also within reasonable error (compressive error range 8 - 44%, off-axis error range 6 - 50%). The excellent performance of the QCT-FEMs with DVC-derived BCs within the current study may partly be attributed to the fact that loading only within the elastic range was performed, simplifying the QCT-FEMs generated, compared to step-wise fracture loading previously performed (Hussein et al., 2018; Jackman et al., 2016). In addition, inherent differences between the vertebra and scapula, and their

296 constitutive equations used to assign material properties may contribute to the performance
297 differences in QCT-FEMs of this study compared to previous vertebral studies. Therefore,
298 although excellent agreement between the QCT-FEM predictions and DVC results were observed
299 within the current study in the shoulder, it is unknown whether these findings can be extrapolated
300 to QCT-based FEMs of other joints.

301 To perform cadaveric experimental loading within a microCT, a secondary objective
302 included the design of a CT-compatible loading device. The robot's ability to generate articular
303 loads within a small working envelope overcame a major design constraint imposed by space
304 restrictions within a CT scanner. Furthermore, controlled loading in 6-dof is a marked
305 improvement over previously developed screw-based CT-compatible devices (Jackman et al.,
306 2016; Martelli and Perilli, 2018; Palanca et al., 2016; Sukjamsri et al., 2015). Precision of the DVC
307 measurements was found not to be affected by the hexapod robot, as errors < 2.5 μm along each
308 Cartesian direction were recorded during the repeated scans procedure further demonstrating the
309 feasibility of the apparatus.

310 For QCT-FEMs with idealized-force BCs, local displacement predictions generally
311 underestimated the experimental results. In addition, computed reaction forces required to displace
312 the virtual platen were much higher in QCT-FEMs with idealized-displacement BCs compared to
313 idealized-force BCs. This may suggest that the QCT-FEMs may have been too stiff due to over-
314 constrained idealized BCs. Only stiffness of the specimen mount (including the PMMA cement)
315 is relevant, since the experimental displacement was measured from microCT rather than from the
316 apparatus itself. Potentially, local DVC displacement measurements could have been applied to
317 the bottom surface of the idealized QCT-FEMs and this may have reduced the observed
318 differences; however, this would require localized displacement measures as an input into the

QCT-FEMs that may not always be attainable. Nonetheless, stiffness of the experimental setup was not accounted for in this study, as the idealized BCs were modelled according to the literature (Chen et al., 2017; Jackman et al., 2016). Now that it has been observed that QCT-FEMs with DVC-derived BCs can in fact replicate experimental displacement measures, future work could include modelling the experimental apparatus to allow for the QCT-FEMs to become more generalizable.

Limitations within the current study should be noted. First, QCT-FEMs were only validated using linear-isotropic material properties subjected to elastic loads. Therefore, further validation is required to investigate failure mechanisms that arise due to loading within the inelastic region. Furthermore, only local displacement measurements and global reaction forces were used to quantify the performance of scapula QCT-FEMs. While strain is a commonly used metric produced by QCT-FEMs to predict failure, experimental strains calculated from microCT-based DVC displacements exhibit higher uncertainties. As the scope of the current study only included evaluating local displacements and global reaction forces, the impact of boundary conditions on other local outcome predictions such as strain was not explored. A Synchrotron light source could be used which may reduce experimental uncertainties (Comini et al., 2019; Palanca et al., 2017); however, this was outside the scope of the current study. Finally, the low sample size (n = 4) of this study is a limitation, which was a product of the complex and time-consuming loading and imaging protocol.

The results of the study demonstrate that errors in local displacements predicted by QCT-FEMs of the shoulder can be minimized using DVC-derived boundary conditions. This work also demonstrated that a novel CT-compatible hexapod robot design was effective for applying 6-dof loading vectors to a scapula while acquiring high-resolution microCT scans in a cone beam

scanner. Combining volumetric imaging with DVC analysis allowed for the ability to evaluate full-field internal displacement predictions generated by the QCT-FEMs that otherwise could not be captured with traditional surface-based measurement techniques (Dahan et al., 2016; Lin et al., 2016). Further development of these methods should be conducted to examine fracture mechanisms.

Acknowledgements

The authors would like to thank Aoife Pucchio for her assistance with data collection. This research was supported by a Post Graduate Scholarship from the Natural Sciences and Engineering Research Council of Canada. Jonathan Kusins and Nikolas Knowles are supported in part by a Transdisciplinary Bone & Joint Training Award from the Collaborative Training Program in Musculoskeletal Health Research at Western University. Enrico Dall'Ara and Melissa Ryan were supported by the Engineering and Physical Sciences Research Council (Grant Number: EP/P015778/1).

References

Allred, J.J., Flores-Hernandez, C., Hoenecke Jr, H.R., D'Lima, D.D., 2016. Posterior augmented glenoid implants require less bone removal and generate lower stresses: a finite element analysis. Journal of shoulder and elbow surgery 25, 823–830. https://doi.org/10.1016/j.jse.2015.10.003

Bay, B.K., Smith, T.S., Fyhrie, D.P., Saad, M., 1999. Digital volume correlation: Three-dimensional strain mapping using X-ray tomography. Exp. Mech. 39, 217–226. https://doi.org/10.1007/BF02323555

Boyin Ding, Stanley, R.M., Cazzolato, B.S., Costi, J.J., 2011. Real-time FPGA control of a hexapod robot for 6-DOF biomechanical testing, in: IECON 2011. Presented at the IECON 2011 - 37th Annual Conference of IEEE Industrial Electronics, Melbourne, AU, pp. 252–257. https://doi.org/10.1109/IECON.2011.6119320

Burkhart, T.A., Andrews, D.M., Dunning, C.E., 2013. Finite element modeling mesh quality, energy balance and validation methods: A review with recommendations associated with the modeling of bone tissue. J Biomech 46, 1477–1488. https://doi.org/10.1016/j.jbiomech.2013.03.022

Chen, Y., Dall′Ara, E., Sales, E., Manda, K., Wallace, R., Pankaj, P., Viceconti, M., 2017. Micro-CT based finite element models of cancellous bone predict accurately displacement once the

boundary condition is well replicated: A validation study. J Mech Behav Biomed Mater 65, 644–651. https://doi.org/10.1016/j.jmbbm.2016.09.014

Comini, F., Palanca, M., Cristofolini, L., Dall'Ara, E., 2019. Uncertainties of synchrotron microCT-based digital volume correlation bone strain measurements under simulated deformation. J Biomech 86, 232–237. https://doi.org/10.1016/j.jbiomech.2019.01.041

Costa, M.C., Tozzi, G., Cristofolini, L., Danesi, V., Viceconti, M., Dall'Ara, E., 2017. Micro Finite Element models of the vertebral body: Validation of local displacement predictions. Plos One 12, 1–18. https://doi.org/10.1371/journal.pone.0180151

Croom, B., Wang, W.-M., Li, J., Li, X., 2016. Unveiling 3D Deformations in Polymer Composites by Coupled Micro X-Ray Computed Tomography and Volumetric Digital Image Correlation. Exp. Mech. 56, 999–1016. https://doi.org/10.1007/s11340-016-0140-7

Croom, B.P., Jin, H., Mills, B., Carroll, J., Long, K., Brown, J., Li, X., 2019. Damage mechanisms in elastomeric foam composites: Multiscale X-ray computed tomography and finite element analyses. Compos Sci Technol 169, 195–202. https://doi.org/10.1016/j.compscitech.2018.11.025

Croom, B.P., Xu, P., Lahoda, E.J., Deck, C.P., Li, X., 2017. Quantifying the three-dimensional damage and stress redistribution mechanisms of braided SiC/SiC composites by in situ volumetric digital image correlation. Scr. Mater 130, 238–241. https://doi.org/10.1016/j.scriptamat.2016.12.021

Dahan, G., Trabelsi, N., Safran, O., Yosibash, Z., 2016. Verified and validated finite element analyses of humeri. J Biomech 49, 1094–1102. https://doi.org/10.1016/j.jbiomech.2016.02.036

Dall'Ara, E., Barber, D., Viceconti, M., 2014. About the inevitable compromise between spatial resolution and accuracy of strain measurement for bone tissue: A 3D zero-strain study. J Biomech 47, 2956–2963. https://doi.org/10.1016/j.jbiomech.2014.07.019

Dall'Ara, E., Peña-Fernández, M., Palanca, M., Giorgi, M., Cristofolini, L., Tozzi, G., 2017. Precision of Digital Volume Correlation Approaches for Strain Analysis in Bone Imaged with Micro-Computed Tomography at Different Dimensional Levels. Front Mater Sci 4, 1–13. https://doi.org/10.3389/fmats.2017.00031

Du, J., Lee, J.-H., Jang, A.T., Gu, A., Hossaini-Zadeh, M., Prevost, R., Curtis, D.A., Ho, S.P., 2015. Biomechanics and strain mapping in bone as related to immediately-loaded dental implants. J Biomech 48, 3486–3494. https://doi.org/10.1016/j.jbiomech.2015.05.014

Gillard, F., Boardman, R., Mavrogordato, M., Hollis, D., Sinclair, I., Pierron, F., Browne, M., 2014. The application of digital volume correlation (DVC) to study the microstructural behaviour of trabecular bone during compression. J Mech Behav Biomed Mater 29, 480–499. https://doi.org/10.1016/j.jmbbm.2013.09.014

Grassi, L., Isaksson, H., 2015. Extracting accurate strain measurements in bone mechanics: a critical review of current methods. J Mech Behav Biomed Mater 50, 43–54. https://doi.org/10.1016/j.jmbbm.2015.06.006

Gupta, S., Van Der Helm, F.C.T., Sterk, J.C., Van Keulen, F., Kaptein, B.L., 2004. Development and experimental validation of a three-dimensional finite element model of the human scapula. Proc Inst Mech Eng H 218, 127–142. https://doi.org/10.1243/095441104322984022

Hussein, A.I., Louzeiro, D.T., Unnikrishnan, G.U., Morgan, E.F., 2018. Differences in Trabecular Microarchitecture and Simplified Boundary Conditions Limit the Accuracy of Quantitative Computed Tomography-Based Finite Element Models of Vertebral Failure. J Biomech Eng 140, 1–11. https://doi.org/10.1115/1.4038609

Jackman, T.M., DelMonaco, A.M., Morgan, E.F., 2016. Accuracy of finite element analyses of CT scans in predictions of vertebral failure patterns under axial compression and anterior flexion. J Biomech 49, 267–275. https://doi.org/10.1016/j.jbiomech.2015.12.004

Knowles, N.K., G. Langohr, G.D., Faieghi, M., Nelson, A., Ferreira, L.M., 2019. Development of a validated glenoid trabecular density-modulus relationship. J Mech Behav Biomed Mater 90, 140–145. https://doi.org/10.1016/j.jmbbm.2018.10.013

Lawless, I.M., Ding, B., Cazzolato, B.S., Costi, J.J., 2014. Adaptive velocity-based six degree of freedom load control for real-time unconstrained biomechanical testing. J Biomech 47, 3241–3247. https://doi.org/10.1016/j.jbiomech.2014.06.023

Lin, Z.X., Xu, Z.-H., An, Y.H., Li, X., 2016. In situ observation of fracture behavior of canine cortical bone under bending. Mater. Sci. Eng. C 62, 361–367. https://doi.org/10.1016/j.msec.2016.01.061

Liu, L., Morgan, E.F., 2007. Accuracy and precision of digital volume correlation in quantifying displacements and strains in trabecular bone. J Biomech 40, 3516–3520. https://doi.org/10.1016/j.jbiomech.2007.04.019

Mao, Q., Su, K., Zhou, Y., Hossaini-Zadeh, M., Lewis, G.S., Du, J., 2019. Voxel-based micro-finite element analysis of dental implants in a human cadaveric mandible: Tissue modulus assignment and sensitivity analyses. J Mech Behav Biomed Mater 94, 229–237. https://doi.org/10.1016/j.jmbbm.2019.03.008

Martelli, S., Perilli, E., 2018. Time-elapsed synchrotron-light microstructural imaging of femoral neck fracture. J Mech Behav Biomed Mater 84, 265–272. https://doi.org/10.1016/j.jmbbm.2018.05.016

Nazarian, A., Müller, R., 2004. Time-lapsed microstructural imaging of bone failure behavior. J Biomech 37, 55–65. https://doi.org/10.1016/S0021-9290(03)00254-9

Oliviero, S., Giorgi, M., Dall'Ara, E., 2018. Validation of finite element models of the mouse tibia using digital volume correlation. J Mech Behav Biomed Mater 86, 172–184. https://doi.org/10.1016/j.jmbbm.2018.06.022

Palanca, M., Bodey, A.J., Giorgi, M., Viceconti, M., Lacroix, D., Cristofolini, L., Dall'Ara, E., 2017. Local displacement and strain uncertainties in different bone types by digital volume correlation of synchrotron microtomograms. J Biomech 58, 27–36. https://doi.org/10.1016/j.jbiomech.2017.04.007

Palanca, M., Cristofolini, L., Dall'Ara, E., Curto, M., Innocente, F., Danesi, V., Tozzi, G., 2016. Digital volume correlation can be used to estimate local strains in natural and augmented vertebrae: An organ-level study. J Biomech 49, 3882–3890. https://doi.org/10.1016/j.jbiomech.2016.10.018

Rice, J., Cowin, S., Bowman, J., 1988. On the dependence of the elasticity and strength of cancellous bone on apparent density. J Biomech 21, 155–168. https://doi.org/10.1016/0021-9290(88)90008-5

Roberts, B.C., Perilli, E., Reynolds, K.J., 2014. Application of the digital volume correlation technique for the measurement of displacement and strain fields in bone: a literature review. Journal of biomechanics 47, 923–934. https://doi.org/10.1016/j.jbiomech.2014.01.001

Schaffler, M.B., Burr, D.B., 1988. Stiffness of compact bone: effects of porosity and density. J Biomech 21, 13–16. https://doi.org/10.1016/0021-9290(88)90186-8

Schneider, C.A., Rasband, W.S., Eliceiri, K.W., 2012. NIH Image to ImageJ: 25 years of image analysis. Nat Methods 9, 671.

Sukjamsri, C., Geraldes, D.M., Gregory, T., Ahmed, F., Hollis, D., Schenk, S., Amis, A., Emery, R., Hansen, U., 2015. Digital volume correlation and micro-CT: An in-vitro technique for measuring full-field interface micromotion around polyethylene implants. J Biomech 48, 3447–3454. https://doi.org/10.1016/j.jbiomech.2015.05.024

Terrier, A., Büchler, P., Farron, A., 2005. Bone–cement interface of the glenoid component: stress analysis for varying cement thickness. Clin Biomech 20, 710–717. https://doi.org/10.1016/j.clinbiomech.2005.03.010

Walker, M.R., Dickey, J.P., 2007. New methodology for multi-dimensional spinal joint testing with a parallel robot. Med Biol Eng Comput 45, 297–304. https://doi.org/10.1007/s11517-006-0158-6

Zauel, R., Yeni, Y.N., Bay, B.K., Dong, X.N., Fyhrie, D.P., 2005. Comparison of the Linear Finite Element Prediction of Deformation and Strain of Human Cancellous Bone to 3D Digital Volume Correlation Measurements. J Biomech Eng 128, 1–6. https://doi.org/10.1115/1.2146001

Zheng, M., Zou, Z., Bartolo, P. jorge D. silva, Peach, C., Ren, L., 2017. Finite element models of the human shoulder complex: a review of their clinical implications and modelling techniques: Finite

Element Models of Human Shoulder Complex. Int J Numer Method Biomed Eng. 33, e02777. https://doi.org/10.1002/cnm.2777

Zhou, Y., Lamberty, M.A.H., Lewis, G.S., Armstrong, A.D., Du, J., 2018. 3D Full-Field Mechanical Measurement of a Shoulder Bone Under Implant Loading, in: TMS Annual Meeting & Exhibition. Springer, pp. 287–293. https://doi.org/10.1007/978-3-319-72526-0_26